

Photoluminescence quenching in compressed MgO nanoparticle systems

Nicolas Siedl^a, David Koller^a, Andreas Kurt Sternig^a, Daniel Thomele^{a,c} and Oliver Diwald^{*a,c}

Received (in XXX, XXX) Xth XXXXXXXXX 20XX, Accepted Xth XXXXXXXXX 20XX

DOI: 10.1039/b000000x

^a *Institute of Particle Technology, Friedrich-Alexander University Erlangen-Nürnberg,
Cauerstraße 4, 91058 Erlangen, Germany;*

^b *Institute of Materials Chemistry, Vienna University of Technology, Getreidemarkt 9 1060 Vienna,
Austria*

^c *Department of Materials Science and Physics, University of Salzburg, Hellbrunnerstrasse 34/ III, A-
5020 Salzburg, Austria*

Fax: +43-662-8044-622; Tel: +43-662-8044-5444; E-mail: oliver.diwald@sbg.ac.at

Key words: transparent ceramics, microstructure of nanopowders, light penetration,
grainboundaries, solid-solid interfaces

Abstract

Efficient use of highly dispersed metal oxides for lighting, energy conversion and catalysis requires knowledge about the impact of density and microstructure of the powders on the optical nanoparticle properties. For MgO nanocube powders we present a combined photoluminescence (PL) and electron paramagnetic resonance (EPR) approach which enables for samples of different aggregation states the quantification of the fractional powder volume that becomes illuminated with UV and Visible light during the PL measurements. Using O₂ as a PL emission quencher and – after light induced exciton separation and oxygen adsorption – as an EPR active adsorbate we observed clear aggregation dependent trends in PL emission quenching that originate from particle-particle contacts. Upon interaction of low coordinated surface elements with the surfaces of adjacent MgO nanocubes, which occur even at powder consolidation levels that escape sorption analysis, the radiative decay of excited surface states become quenched down to 15% of the original intensity. Our results underline the critical role of microstructure and aggregation state of the nanoparticle ensemble with respect to spectroscopic properties and related adsorption induced changes.

Introduction

The fabrication of electronic devices containing nanocrystalline components and catalyst design are two examples where controlled microstructure manipulation on the atomic level plays an outstanding role.¹ Based on particle systems as the primary components for microstructure formation new materials design approaches have emerged. Functional nanocrystalline materials with aggregation levels varying between that of a loose nanoparticle agglomerate to that of a dense polycrystalline ceramic can be engineered through powder compression and subsequent sintering procedures.^{2,3} The properties of such materials depend on the size, chemical composition and structure of constituent grains, as well as the nature of interfacial regions between grains and intergranular pores.⁴⁻⁷ However, analyzing and controlling abundance and properties of interfacial regions in nanocrystalline oxides is extremely difficult and poses a major challenge to the design of high performance functional materials. Interfacial regions in MgO may gain substantial influence with respect to the materials properties of the entire particle ensemble. Elastic properties were found to be markedly affected by the nature of grain boundary networks.⁸ Relevant for the field of heterogeneous catalysis it is expected that structurally disturbed zones at the grain boundaries areas in consolidated powders of MgO polycrystals exhibit increased surface basicity.⁹ The significant increase of surface basicity yielded a major enhancement of catalytic activity as measured by Knoevenagel condensation or transesterification reactions.¹⁰

It was found that compression of ensembles of small MgO particles and – concomitantly – the increase of interfacial contacts between them can give rise to new optical features¹¹ as well as to the depletion or enhancement of features which are linked to free particle surfaces. In order to account for related trends it is necessary to quantitatively assess the optical properties of an entire particle ensemble. This is a challenging task since highly dispersed particle powders

exhibit enhanced reflectivity. The penetration depth of photoluminescence (PL) excitation and emission light, for example, strongly depends on the state of aggregation and, thus, on porosity and concentration of particle-particle interfaces in the respective sample volume (Figure 1).

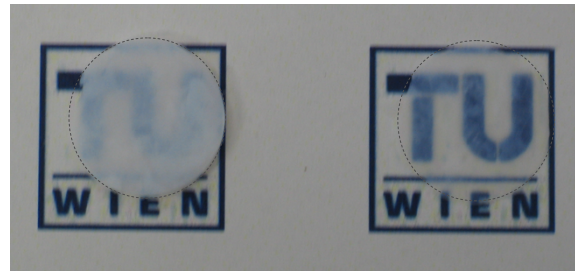


Figure 1: Light scattering effects of uncompressed (left) and compressed powder pellets (right, same amount of powder). The porous microstructure of compressed MgO particle powders is responsible for the opaque materials appearance. Particle powder compression shifts the pore size distribution curve to values below the wavelength of visible light.¹² The significant increase in the transmission of visible light (i.e. in the translucence) is demonstrated for a pellet with a relative powder density of 50 % (right side) relative to the density of a MgO single crystal ($\rho = 3580 \text{ kg}\cdot\text{m}^{-3}$).

From a practical perspective, the controlled generation and the precise engineering of nanoparticle interfaces are important for many applications. For most high surface area directed applications which involve adsorption processes and surface reactivity it is important to keep the concentration of solid-solid interfaces and grain boundaries low. For ceramics, on the other hand, it is necessary to transform loose powders into compacted solids and to subsequently subject these compacts to thermal treatment. Sintering is a critical part of ceramics processing and starts with an assembly of contacting particles.² Initial contacts range from point contacts to highly deformed interfaces. With sintering the contacts grow in size,

and in the initial stage there is extensive loss of surface area. In parallel to these transformations, the structure of the residual pores becomes rounded and the originally discrete particles are less evident. The dramatic impact of such microstructural changes on the nanometer scale on large-scale properties is well illustrated by the development of transparent ceramics. Residual porosity in wide band gap materials like Al_2O_3 , ZrO_2 or MgO leads to substantial loss of visible light transmission via light scattering at the oxide-air interface (Figure 1).¹³⁻¹⁵

MgO nanocube ensembles have been the subject of numerous previous investigations and are perhaps one of the best understood ceramic nanomaterials.¹⁶⁻¹⁹ In previous work, a variety of spectroscopic techniques²⁰⁻²⁵, as well as first-principles theoretical calculations²⁶⁻²⁹ have been used to investigate the electronic properties of MgO nanocubes formed by the controlled combustion of magnesium vapor. UV diffuse reflectance spectroscopy reveals two absorption bands far below the bulk absorption threshold of MgO which have been attributed to corner (4.6 eV) and edge sites (5.2 eV).¹¹ Photoluminescence spectroscopy detects two closely spaced photoemission bands at 3.2 eV and 3.4 eV that result from photoexcitation of corners and edges, respectively.³⁰ While it was usually assumed that photons with sub-band-gap energy exclusively excite low coordinated surface sites more recent studies recognized the importance of the interactions between nanocrystals and contributed to a more complete description of metal oxide nanoparticle powders. We identified a PL emission process at 2.5 eV that is linked to nanocube interfaces.¹² First principles calculations provide plausible candidates for both light absorbing and emitting sites which involve different interface features.^{28,27} It was found that interfaces between nanocube edges and terraces induce a significant electrostatic perturbation of the interfacial electronic states leading to exciton generation and luminescence at lower energies than those related to corners and edges of MgO nanocubes.¹²

The aim of the present study is to describe in a systematic and quantitative way how interfacial contacts between MgO nanocubes inside a given nanoparticle ensemble affect surface excited states. Obtained insights should methodologically advance the investigation of optical property changes associated with solid-solid interfaces in strongly scattering particle systems. Respective characterization work is motivated by the fact that solid-solid interfaces do interact with other point defects, impact radiation damage evolution³¹⁻³³, mass transport and sintering^{2,34}, adsorption on nanocrystalline materials⁴, and catalysis in general.^{9,10,35}

Experimental

MgO nanocube powder synthesis, compression and thermal activation

For the purpose of present study we made use of four MgO nanocube ensemble types at different states of pressure induced aggregation and, thus, concentrations of solid-solid interfaces. Structural, microstructural and the general spectroscopic properties were described elsewhere¹¹ and are briefly summarized in Table 1.

Table 1: Nanocrystalline MgO pellets produced by applying different uniaxial pressures. The table contains the samples' relative densities, surface and interface areas.

Sample	Pressure / Pa	Relative density ^a	$S_{\text{BET}} / \text{m}^2 \cdot \text{g}^{-1}$	Interface area ^b / $\text{m}^2 \cdot \text{g}^{-1}$
MgO		$\rho_{\text{MgO}} / \%$		
RD 0.01	0	< 1	303 ± 30	0
RD 0.15	$5 \cdot 10^7$	15	292 ± 29	0
RD 0.30	$1 \cdot 10^8$	30	163 ± 16	0
RD 0.50	$1.7 \cdot 10^8$	50	108 ± 10	99

^a The relative density of the pellet is given as a fraction of the density of a MgO single crystal ($3580 \text{ kg} \cdot \text{m}^{-3}$)

^b The interface area between nanocubes increases with relative density at the expense of surface area. For its determination we used the difference between the calculated value which was derived from the Scherrer equation (crystallite domain size) and the measured surface area S_{BET} obtained via application of the BET- model. Further details and assumptions related to this approach are provided in reference [12].

For the production of MgO nanocubes we use a chemical vapor synthesis (CVS) procedure corresponding to the controlled evaporation and subsequent oxidation of alkaline earth metals under reduced pressure.¹¹ After production, the MgO nanocrystal powder is transferred into quartz glass cells, which allow one to perform thermal activation of the nanocrystal powders in defined gas atmospheres. To obtain well-defined cubic MgO nanocrystals, the as-prepared MgO powder is cleaned of organic contaminants by heating to 1123 K at a rate of 5 K min^{-1} and exposing to molecular oxygen at this temperature (10 mbar). Then, the sample temperature is raised to 1173 K at pressures $p < 5 \cdot 10^{-6}$ mbar and kept at this temperature for 5 h until full dehydroxylation of the sample surface is achieved. This procedure forms low-density powders (less than 1% of the bulk MgO density, $\rho_{\text{MgO}} = 3580 \text{ kg m}^{-3}$), and transmission electron microscopy (TEM) demonstrates they consist of agglomerated cubic nanocrystals. A defined mass of the powder is transferred into a 0.05 cm^3 cavity and a hydraulic press is used to compact the powder. By varying the pressure applied, compressed powders of densities up to 50% can be obtained in a controlled and reproducible way (Table 1). After pressing, the MgO pellets were subjected to oxidation in 10 mbar oxygen at 1123 K for 10 min and an additional vacuum annealing procedure at 1173 K for 5 h at pressures below $5 \cdot 10^{-6}$ mbar to achieve perfect sample dehydroxylation.

Photoluminescence measurements

Room temperature photoluminescence (PL) measurements were carried out using Suprasil quartz glass tubes which guarantee vacuum conditions better than $5 \cdot 10^{-6}$ mbar. (The same cells were employed for electron paramagnetic resonance (EPR) measurements.) PL spectra were measured with a Perkin-Elmer LS 50B system and a pulsed Xe discharge lamp served as excitation source as well as irradiation source for UV-induced surface chemistry (generation of oxygen radicals, see below). The light power was specified by Perkin Elmer to be equivalent to 20 kW for 8 μ s pulse duration. Further details about the optical properties of MgO nanocube powders including the spectral data of the used instruments are provided in reference [11].

Electron Paramagnetic Resonance measurements

For EPR measurements, the powder sample was contained within the above mentioned Suprasil quartz glass tube connected to an appropriate high vacuum pumping system with a base pressure $p < 10^{-6}$ mbar. This allows for thermal sample activation and UV irradiation in situ. A 300 W Xe lamp (Oriel) was used as UV source. The light beam was passed through a water filter to exclude IR contributions from the excitation spectrum and a bandpass filter (265 FS 10-50 (P228-01)) to set an irradiation wavelength of $\lambda = 270$ nm. Light power was measured with a bolometer (International Light). It was held constant at $P_{\text{irr}} = 0.2 \text{ mW} \cdot \text{cm}^{-2}$ at $\lambda = 270$ nm throughout all experiments. During UV exposure, the samples were held at a temperature of $T = 293$ K. For EPR measurements the samples were cooled to $T = 140$ K. X-band EPR measurements were performed on a Bruker EMX Micro spectrometer using a Bruker ER 4119 HS resonator. For measurements at $T = 140$ K an ER 4131 VT variable-

temperature accessory was used. EPR computer simulations were done using the SIM 14S program. The g values were determined on the basis of a DPPH standard.

Results and Discussion

1. Photoluminescence quenching by O₂

Surface excitons are well suited quantitative probes for the characterization of optical powder properties. The photoluminescence emission related to the photoexcitation of MgO nanocube corners ($h\nu = 4.6$ eV, quantum yield $\Phi = 0.05$) and nanocube edges ($h\nu = 5.4$ eV, quantum yield $\Phi = 0.20$) are characterized by two closely spaced emission bands at 3.2 eV and 3.4 eV, respectively.¹¹ PL emission from MgO nanoparticle surfaces competes with nonradiative pathways of surface exciton deactivation. In Figure 2a the impact of molecular oxygen as a photoluminescence quencher³⁶ is demonstrated for the emission process that originates from the photoexcitation of MgO nanocube edges with $h\nu = 5.4$ eV light. Figure 2b shows the O₂ pressure dependent relative emission intensity decreases corresponding to the two processes of radiative surface exciton deactivation.³⁰

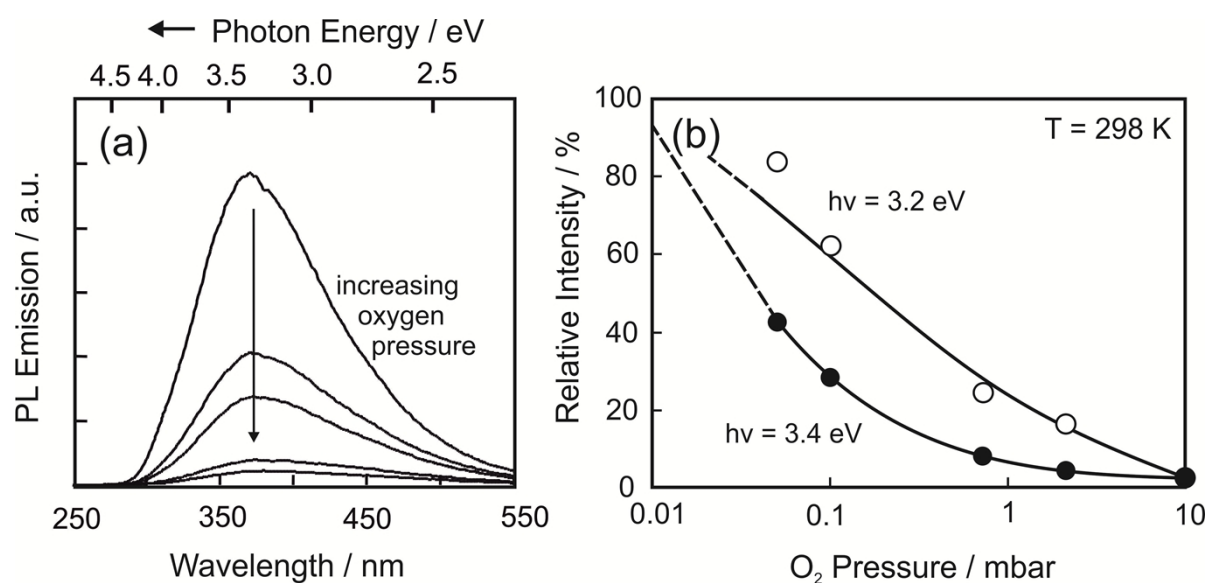


Figure 2: Relative PL emission band intensity development on MgO nanocube samples with increasing O₂ pressure. The spectra shown in (a) correspond to the emission process which is

linked to the photoexcitation of MgO nanocube edges ($h\nu_{\text{EXC}} = 5.4 \text{ eV}$). Figure 2b plots relative PL intensity decrease in the oxygen partial pressure range $0.05 \text{ mbar} \leq p \leq 10 \text{ mbar}$. The values related to relative intensity = 100% correspond to the PL emissions acquired on a MgO powder sample at $p < 5 \cdot 10^{-6} \text{ mbar}$.

2. Electron paramagnetic resonance: UV induced oxygen radical formation

In addition to collisional PL quenching of surface excited states by O_2 molecules impinging from the gas phase (Figure 2) there exists also exciton splitting.^{31,37} This process corresponds to the decomposition of a surface excited state into a hole and an ejected electron.³⁸ Being subject to the temperature of the powder this either leads on MgO surfaces to O_3^- (Figure 3a and b) or O^- (Figure 3c) with characteristic EPR signatures of hole acceptors.³⁹

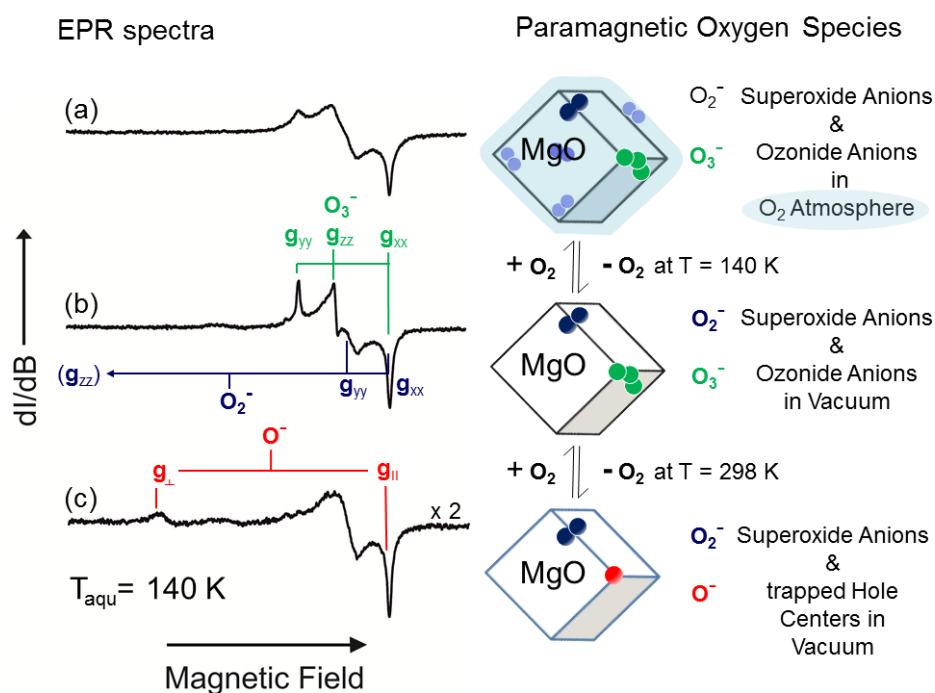


Figure 3: EPR spectra related to uncompressed MgO nanocrystal samples after UV exposure to 4.6 eV light in O_2 atmosphere. (a) Spectrum acquired in the presence of O_2 (1 mbar), (b) after subsequent pumping at the spectrum acquisition temperature $T = 140 \text{ K}$ and (c) after intermediate warming to room temperature

Figure 3a shows a characteristic EPR spectrum which was acquired after the powder had been exposed to monochromatic UV light ($h\nu = 4.6$ eV) in O_2 atmosphere and which was then cooled from $T = 298$ K to $T = 140$ K. The three component signal is associated with a specific surface ozonide anion type at oxygen terminated corners (first and second row of Figure 3).³⁹ Upon pumping the sample volume down to $p < 10^{-6}$ mbar the spectral features become more distinct (Figure 3b). This effect is attributed to the removal of physisorbed paramagnetic O_2 molecules which can interact with paramagnetic surface species via spin-exchange interaction and lead to O_2 pressure dependent signal broadening (Figure 3a). In addition to the O_3^- specific g factors (Figure 3b and Table 2) an additional feature at $g = 2.008$ related to the g_{yy} component of superoxide anions O_2^- emerges.^{39,40} Its presence provides evidence for an efficient transfer of surface trapped electrons to molecular oxygen. Consistent with an earlier study³⁹, sample warming to temperatures above $T = 200$ K decomposes the ozonide signal upon release of O_2 molecules into the gas phase and the emergence of a two component EPR signal with $g_{\perp} = 2.036$ and $g_{\parallel} = 2.002$ (Table 2) as EPR spectroscopic fingerprint of trapped hole centers located at an oxygen terminated corner.

Table 2: EPR parameters of oxygen radicals detected with EPR spectroscopy at $T=140$ K (Figure 3)

O^-	$g_{\perp} = 2,0358$	$g_{\parallel} = 2,0023$	
O_2^-	$g_{yy} = 2,0080$	$g_{xx} = 2,0023$	
O_3^-	$g_{zz} = 2,0103$	$g_{yy} = 2,0157$	$g_{xx} = 2,0023$

3. Determination of the fractional illuminated powder volume V_i by combined PL and EPR measurements

We prepared MgO nanocube powder samples with different levels of particle aggregation (Table 1). Since light scattering and, consequently, the penetration depth of light is subject to aggregation state inside the illuminated particle volume (Figure 1)¹¹, the integral intensity values of PL emission need to be corrected for fractional powder volume that is effectively illuminated. For this purpose we developed a combined PL and EPR spectroscopic approach that addresses the effect of O₂ adsorption on nonradiative exciton annihilation (PL quenching, Figure 2) and determined at the same time the evolution of oxygen radicals emerging from exciton separation and interfacial charge transfer (EPR, Figure 3b).

The combined EPR and PL measurements were organized in the following way: for each type of powder sample - compressed or uncompressed - we determined with EPR spectroscopy the maximum number of spins related to O₃⁻ ions inside the entire powder sample after exposure to UV excitation in oxygen atmosphere (Figure 3b). For this purpose the sample cell, that was connected to the a flexible high vacuum tubing, was shaken and rotated for a couple of times in order to achieve sufficient intermixture between the different powder regions. For determining the concentration of O₃⁻ ions per sample mass we used a previously established quantification approach which is outlined in detail in references [41,42]. By accounting for the average particle size¹¹ these values were then translated into EPR intensities/ particle.

In a second step we exposed the powder samples inside the PL/ EPR quartz glass tubes simultaneously to oxygen ($p(\text{O}_2) = 1 \text{ mbar}$) and UV light using the excitation source of the PL spectrometer system ($h\nu = 4.6 \text{ eV}$ and with light power of $0.03 \text{ mW}\cdot\text{cm}^{-2}$).¹¹ In the course of this type of experiment which corresponds to the typical PL measurement we kept the same

position and orientation of the sample cell with respect to the light source. After that and without breaking the vacuum or – in case of oxygen gas containing sample volumes – without changing the gas phase composition the sample cells were connected to the high vacuum rack of the EPR spectrometers system and cooled to 140 K for subsequent EPR spectrum acquisition (Figure 3a). Spin concentrations related to photogenerated O_3^- ions were determined via the peak to peak amplitudes of the distinct EPR signals in conjunction with double integration of the signal after evacuation (Figure 3b). As a result we obtained the fractional illumination volume V_i , i.e. the percentage of particles that can be reached by UV excitation and emit light during the PL measurements (Figure 2), for the different compressed particle samples (Table 3).

Table 3: Nanocrystalline MgO pellets and the *correction factors* for the fractional illuminated volume V_i .

Sample	Relative density $\rho_{MgO}^a / \%$	Fractional illumination volume ^b $V_i / \%$
MgO (RD 0.01)	< 1	28 ± 3
MgO (RD 0.15)	15	20 ± 2
MgO (RD 0.30)	30	46 ± 5
MgO (RD 0.50)	50	28 ± 3

^a the relative density of the pellet is given as a fraction of the density of a MgO single crystal ($3580 \text{ kg}\cdot\text{m}^{-3}$)

^b the fractional illumination volume corresponds to the ratio number of illuminated particles / total number of particles (or volume of illuminated particles/ total sample volume)

Significant differences in the V_i values can be concluded from Table 3. Their non-monotonous development with increasing level of pressure induced consolidation is explained by the fact that various microstructure related factors, such as grain size growth, pore size distribution and the amount of solid-solid interfaces contribute to the overall scattering characteristics of each sample in different ways.⁴³

Typical UV exposure times of less than 3 hours were sufficient to achieve for a given sample cell orientation the maximum radical concentration inside a fractional powder volume. Figure 4 demonstrates for a compressed MgO nanoparticle powder (MgO RD 0.50) with a relative powder density of 50% that only a part of the entire sample volume, i.e. the coloured region in the image of Figure 4a, is accessible to UV light. Clearly visible to the eye, the brownish powder part corresponds to an optical absorption feature with a maximum at 2.9 eV plotted in the UV diffuse reflectance spectrum (Figure 4b).

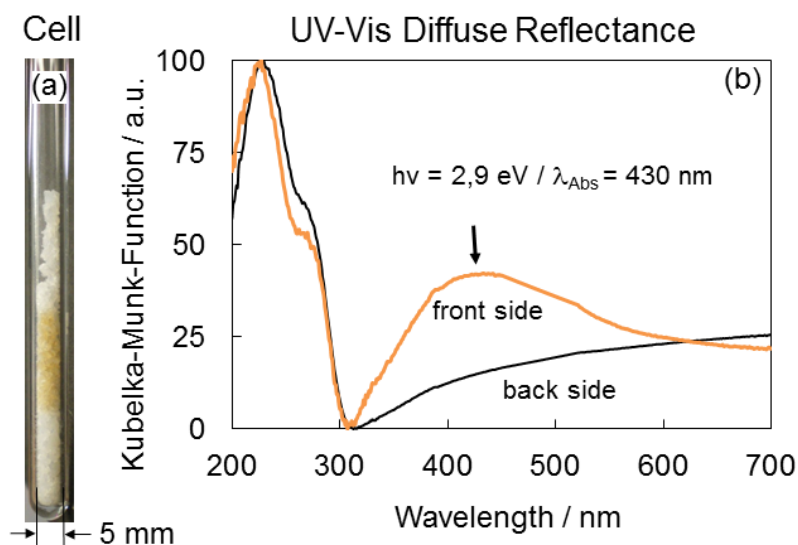


Figure 4: Powder coloration of compressed MgO nanoparticle samples after UV exposure in O_2 atmosphere (1 mbar). The brown coloured powder region at the front side of the quartz glass cell in image (a) corresponds to the broad absorption in the visible light region (brown line) of the diffuse reflectance spectrum in (b). As a reference, the black line corresponds to

the UV-Vis diffuse reflectance spectrum of the sample backside which was not reached by UV light.

In terms of oxygen partial pressure and temperature dependent stability this effect displays similar characteristics as the EPR fingerprints of O^- radicals which start to degrade upon pumping at temperatures above $T = 373$ K. Consequently, we attribute this absorption feature to surface trapped hole centers rather than to O_3^- ions as their oxygen adducts.^{44,45}

4. Particle aggregation dependent PL emission yield trends

The ionic character of chemical bonding in MgO implies a strong dependence of the electronic structure on the local coordination of surface ions. The question arises to what extent interactions between nanocube corners and edges on adjacent particles do influence their electronic structure and in particular the fate of associated surface excitons. Comparison of Figure 5a (uncorrected data) with those corrected for light scattering loss (Figure 5b) points to the importance to account for the number of nanocubes reached by UV light as well as for pressure induced microstructural changes inside the powders. After correction, we observe a dramatic decrease in PL emission already for a slightly compressed sample such as MgO RD 0.15 (Table 1 and Figure 5b).

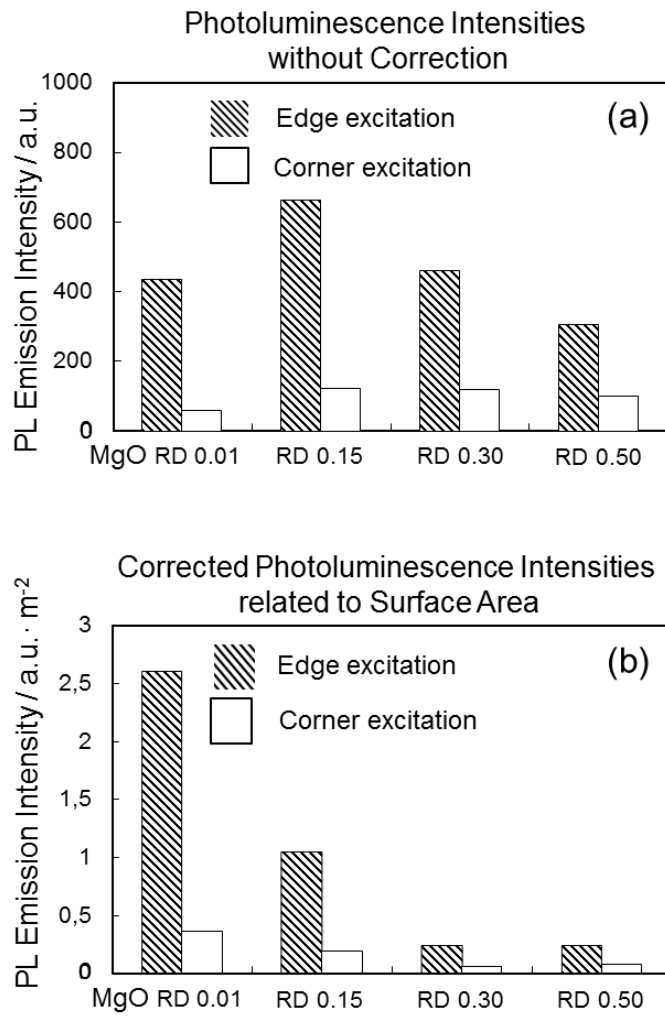


Figure 5: PL emission intensities of loose MgO nanocube powders in comparison to consolidated samples (MgO RD 0.01 versus MgO RD 0.15 to RD 0.50). While panel (a) shows the obtained intensity values panel (b) plots the values which were corrected for changes in the fractional illumination volume (Table 3).

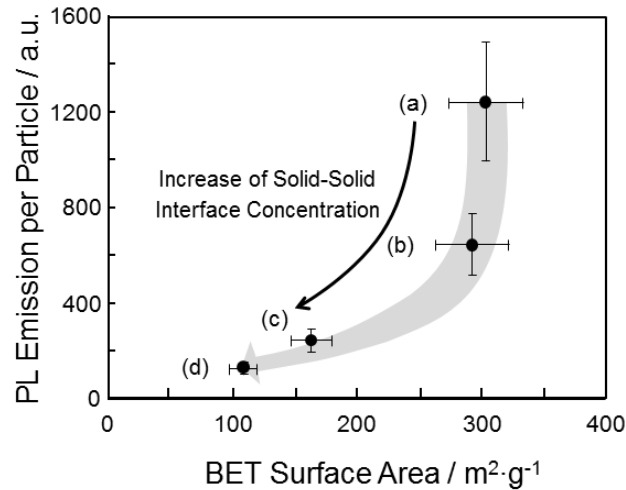


Figure 6: Corrected intensity values related to the PL emission originating from the photoexcitation of MgO nanocube edges ($h\nu_{\text{EXC}} = 5.4$ eV). The associated specific surface areas were determined using the BET model for the analysis of N_2 sorption isotherms (S_{BET}). The points labeled (a), (b), (c) and (d) are associated with the MgO samples RD 0.01, 0.15, 0.30 and 0.50, respectively.

Figure 6 underlines an important point concerning the sensitivity of radiative exciton deactivation towards the mutual distance between particles. Comparison of the PL emission intensities observed for a loose MgO nanoparticle powder sample MgO RD 0.01, Figure 6a) with that of a compressed MgO powder of low relative density (MgO RD 0.15, Figure 6b) reveals a significant PL emission intensity decrease. The high specific surface areas of the two samples, however, are comparable (Table 1). In other words, sorption analysis excludes a significant loss of surface area which is accessible to N_2 molecules. This indicates that the electronic structure of i) oxygen terminated corners and/ or of ii) MgO nanocube edges which guide excitons from the excitation sites to the emission sites³⁸ become significantly perturbed as PL emission sites upon low levels of aggregation.

For grain boundaries in ionic metal oxides theory predicts that the boundary structure has an

important impact on point defect-boundary interactions.⁴⁶ Furthermore, as a particularity of nanocrystalline ceramics, the small average crystallite size leads to a situation where the volume fraction of interfacial regions between the randomly oriented crystallites can become as high as that of the bulk. Consequently, a significant fraction of the material consists of interfaces and these may induce particular functions to the integral solid. A recent study in the field of heterogeneous catalysis revealed that densification of MgO aerogel derived nanostructures increases their acid-base properties by a factor of 1.8 to 3.⁹ These experimental findings were rationalized by the hypothesis that coordinatively unsaturated surface ions near the grain boundaries, i.e. at the distance of the first four atomic layers from the geometrical contact plane, become displaced upon consolidation. Resulting occupied states in the band gap alter the materials' catalytic activity. Apart from the difference in particle synthesis – gas phase synthesis as a solvent free technique versus the sol-gel based fabrication of aerogels – the here employed particle system with a relative density of 15% (MgO RD 0.15, Table 1, Figure 6b) exhibits a significantly lower level of consolidation than those discussed in reference.⁹ PL spectroscopy is a particularly sensitive technique and well-suited for the characterization of oxide surfaces relative to adsorption, catalysis, and photocatalysis. As an example adsorption processes which involve submonolayer surface coverages of hydrogen can be tracked on nanocrystalline MgO systems.²⁵ Here we show that only minor changes in the aggregation level have a strong effect on the electronic properties of MgO corners and edges. The non-radiative annihilation of surface excitons clearly indicates surface electronic structure changes upon particle powder compression. When nanocrystalline metal oxides are employed as catalysts or as bare catalyst supports particle consolidation is usually performed to achieve sufficient mechanical strength of the material against gas stream induced loss of particles. So far neglected structural features such as particle contacts which may lead to distinct spectroscopic features¹¹ may also deplete those associated with specific surface elements of free particle surfaces and potentially affect the chemical reactivity of the entire

particle ensemble.

Sample preparation for materials characterization is connected to another important aspect related to particle-particle interfaces. In order to perform spectroscopic measurements in the transmission mode, nanoparticle powders are usually pressed into pellets, inevitably generating nanocrystal interfaces. A deeper understanding of how interfaces affect optical properties may open the way to using optical spectroscopy as a probe of the electronic properties of interfaces between nanocrystals, which are thought to be important for effects such as magnetism in nanopowders⁴⁷ and for understanding the dynamics of electrons and holes under irradiation. More research in experiment and theory is needed to address the complex problem of interface activity of consolidated high surface area materials.

Summary

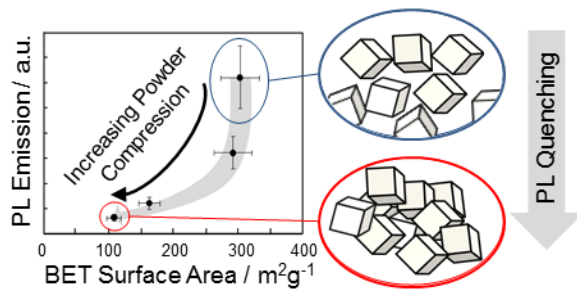
Electron paramagnetic resonance was used to measure the concentration of oxygen radicals which emerge from UV excitation of MgO nanocube powders in O₂ atmosphere. At the same time we tracked the O₂ dependent PL quenching effects and employed the combination of both spectroscopic techniques to determine the fractional powder volume accessible for UV light of metal oxide nanoparticles at different states of aggregation. On this basis we realized for compressed MgO nanocube ensembles a disproportionate reduction of PL intensity with increasing level of consolidation. Even at concentrations of particle contacts that are below a level that can be tracked by N₂ sorption analysis they critically affect the the optical materials properties. From a methodological point of view the here reported approach provides a base for a correct determination of the number of illuminated particles and to reliably compare PL emission trends that originate from the photoexcitation of corners and edges in compressed nanocube powders.¹¹ Related impact of particle-particle contacts on surface excitonic transitions in insulating polycrystalline metal oxides is relevant to radiation damage evolution,

mass transport and sintering and adsorption on nanocrystalline materials.

Acknowledgments

The authors thank Deutsche Forschungsgemeinschaft (DFG) for funding this project within the Research Training Group 1161 “Disperse Systems for Electronic Applications”. A.S. and O.D. gratefully acknowledge support from the Austrian Fonds zur Förderung der Wissenschaftlichen Forschung FWF-PI312 (ERA Chemistry). We like to thank Dr. Thomas Berger for his critical comments on this manuscript and related discussions.

TOC graphic



References

- 1 H. Gleiter, *Acta Materialia*, 2000, **48**, 1–29.
- 2 R. M. German, *Sintering theory and practice*, Wiley, New York, 1996.
- 3 A. R. Studart, U. T. Gonzenbach, E. Tervoort and L. J. Gauckler, *Journal of the American Ceramic Society*, 2006, **89**, 1771–1789.
- 4 R. Richards, W. Li, S. Decker, C. Davidson, O. Koper, V. Zaikovski, A. Volodin, T. Rieker and K. J. Klabunde, *Journal of the American Chemical Society*, 2000, **122**, 4921–4925.
- 5 S. Kim, X. Wang, C. Buda, M. Neurock, O. B. Koper and J. T. Yates, JR., *Journal of Physical Chemistry C*, 2009, **113**, 2219–2227.
- 6 P. Kubiak, T. Fröschl, N. Hüsing, U. Hörmann, U. Kaiser, R. Schiller, C. K. Weiss, K. Landfester and M. Wohlfahrt-Mehrens, *Small*, 2011, **7**, 1690–1696.
- 7 T. Fröschl, U. Hörmann, P. Kubiak, G. Kučerová, M. Pfanzelt, C. K. Weiss, R. J. Behm, N. Hüsing, U. Kaiser, K. Landfester and M. Wohlfahrt-Mehrens, *Chem. Soc. Rev.*, 2012, **41**, 5313.
- 8 H. Marquardt, A. Gleason, K. Marquardt, S. Speziale, L. Miyagi, G. Neusser, H.-R. Wenk and R. Jeanloz, *Physical Review B - Condensed Matter and Materials Physics*, 2011, **84**.
- 9 D. Vingurt, D. Fuks, M. V. Landau, R. Vidruk and M. Herskowitz, *Phys. Chem. Chem. Phys.*, 2013, **15**, 14783.
- 10 R. Vidruk, M. V. Landau, M. Herskowitz, M. Talianker, N. Frage, V. Ezersky and N. Froumin, *Journal of Catalysis*, 2009, **263**, 196–204.
- 11 A. Sternig, S. Stankic, M. Müller, N. Siedl and O. Diwald, *Nanoscale*, 2012, **4**, 7494–7500.
- 12 A. Sternig, D. Koller, N. Siedl, O. Diwald and K. McKenna, *Journal of Physical Chemistry C*, 2012, **116**, 10103–10112.
- 13 S. Wang, J. Zhang, D. Luo, F. Gu, D. Tang, Z. Dong, G. Tan, W. Que, T. Zhang, S. Li and L. Kong, *Progress in Solid State Chemistry*, 2013, **41**, 20–54.
- 14 T. R. Hinklin, S. C. Rand and R. M. Laine, *Adv. Mater.*, 2008, **20**, 1270–1273.
- 15 A. Krell, J. Klimke and T. Hutzler, *Optical Materials*, 2009, **31**, 1144–1150.
- 16 M. Winterer, *Nanocrystalline Ceramics: Synthesis and Structure*, 2002.
- 17 M. Winterer and H. Hahn, *Zeitschrift fuer Metallkunde/Materials Research and Advanced Techniques*, 2003, **94**, 1084–1090.
- 18 J. L. Boldu O., L. A. Boatner and M. M. Abraham, *Journal of the American Ceramic Society*, 1990, **73**, 2345–2359.
- 19 G. W. Steadman, J. R. Brewster, J. D. Budai and L. A. Boatner, in *Materials Research Society Symposium Proceedings*, 1993, vol. 286, pp. 33–38.
- 20 E. Garrone, A. Zecchina and F. S. Stone, *Philos. Mag. B*, 1980, **42**, 683–703.
- 21 G. Spoto, E. N. Gribov, G. Ricchiardi, A. Damin, D. Scarano, S. Bordiga, C. Lamberti and A. Zecchina, *Progress in Surface Science*, 2004, **76**, 71–146.
- 22 G. Pinarello, C. Pisani, A. D'Ercole, M. Chiesa, M. C. Paganini, E. Giamello and O. Diwald, *Surface Science*, 2001, **494**, 95–110.
- 23 M.-L. Bailly, G. Costentin, H. Lauron-Pernot, J. M. Krafft and M. Che, *Journal of Physical Chemistry B*, 2005, **109**, 2404–2413.
- 24 T. Berger, M. Sterrer, O. Diwald and E. Knözinger, *Journal of Physical Chemistry B*, 2004, **108**, 7280–7285.
- 25 M. Müller, S. Stankic, O. Diwald, E. Knözinger, P. V. Sushko, P. E. Trevisanutto and A. L. Shluger, *Journal of the American Chemical Society*, 2007, **129**, 12491–12496.
- 26 P. V. Sushko and A. L. Shluger, *Surface Science*, 1999, **421**, L157.
- 27 K. P. McKenna and A. L. Shluger, *Physical Review B - Condensed Matter and Materials Physics*, 2009, **79**, 224116.

- 28 K. P. McKenna, P. V. Sushko and A. L. Shluger, *Journal of the American Chemical Society*, 2007, **129**, 8600–8608.
- 29 S. Stankic, M. Cottura, D. Demaille, C. Noguera and J. Jupille, *Journal of Crystal Growth*, 2011, **329**, 52–56.
- 30 A. Sternig, M. Müller, M. McCallum, J. Bernardi and O. Diwald, *Small*, 2010, **6**, 582–588.
- 31 K. M. Beck, A. G. Joly, O. Diwald, S. Stankic, P. E. Trevisanutto, P. V. Sushko, A. L. Shluger and W. P. Hess, *Surface Science*, 2008, **602**, 1968–1973.
- 32 K. M. Beck, M. Henyk, C. Wang, P. E. Trevisanutto, P. V. Sushko, W. P. Hess and A. L. Shluger, *Physical Review B - Condensed Matter and Materials Physics*, 2006, **74**, 045404.
- 33 A. L. Shluger, J. L. Gavartin, M. A. Szymanski and A. Marshall Stoneham, *Nuclear Instruments and Methods in Physics Research, Section B: Beam Interactions with Materials and Atoms*, 2000, **166**, 1–12.
- 34 J. Rankin and L. A. Boatner, *Journal of the American Ceramic Society*, 1994, **77**, 1987–1990.
- 35 C. A. Cadigan, A. R. Corpuz, F. Lin, C. M. Caskey, K. B. H. Finch, X. Wang and R. M. Richards, *Catal. Sci. Technol.*, 2013, **3**, 900.
- 36 M. Anpo, S. Dzwigaj and M. Che, *Advances in Catalysis*, 2009, **52**, 1–42.
- 37 A. G. Joly, M. Henyk, K. M. Beck, P. E. Trevisanutto, P. V. Sushko, W. P. Hess and A. L. Shluger, *Journal of Physical Chemistry B*, 2006, **110**, 18093–18096.
- 38 O. Diwald, M. Sterrer, E. Knözinger, P. V. Sushko and A. L. Shluger, *Journal of Chemical Physics*, 2002, **116**, 1707–1712.
- 39 M. Sterrer, T. Berger, O. Diwald, E. Knözinger and A. Allouche, *Top Catal*, 2007, **46**, 111–119.
- 40 *While the associated g_{xx} component is buried in the EPR signal of the surface ozonide, the g_{zz} component in the low magnetic field region was not resolved under the present experimental conditions.*
- 41 N. Siedl, S. O. Baumann, M. J. Elser and O. Diwald, *Journal of Physical Chemistry C*, 2012, **116**, 22967–22973.
- 42 M. J. Elser and O. Diwald, *Journal of Physical Chemistry C*, 2012, **116**, 2896–2903.
- 43 These experiments were performed once in each case. On the basis of the reproducibility of the combined PL and EPR measurements using different sample charges and powder compression steps, we identified an overall error of +/- 10%. Consequently, the error associated with the determination of the fractional volume (Table 3) must be smaller than that. Thus, the variations of the V_i values between MgO RD 0.01 to RD 0.5 have to be taken as significant differences.
- 44 M. Che and A. J. Tench, *Advances in Catalysis*, 1982, **31**, 77–133.
- 45 M. Che and A. J. Tench, *Advances in Catalysis*, 1983, **32**, 1–148.
- 46 B. P. Uberuaga, X.-M. Bai, P. P. Dholabhai, N. Moore and D. M. Duffy, *J. Phys.: Condens. Matter*, 2013, **25**, 355001.
- 47 M. Stoneham, *J. Phys.: Condens. Matter*, 2010, **22**, 74211.